Acta Oceanol. Sin., 2015, Vol. 34, No. 7, P. 89–96
DOI: 10.1007/s13131-015-0660-5
http://www.hyxb.org.cn
E-mail: hyxbe@263.net

Impact of rain-induced sea surface roughness variations on salinity retrieval from the Aquarius/SAC-D satellite

MA Wentao[1, 2], YANG Xiaofeng[2]*, YU Yang[2], LIU Guihong[2], LI Ziwei[2], JING Cheng[2]

[1] College of Physical and Environmental Oceanography, Ocean University of China, Qingdao 266100, China

[2] State Key Laboratory of Remote Sensing Science, Institute of Remote Sensing and Digital Earth, Chinese Academy of Sciences, Beijing 100101, China

Received 8 October 2014; accepted 2 February 2015

Abstract

Rainfall has two significant effects on the sea surface, including salinity decreasing and surface becoming rougher, which have further influence on L-band sea surface emissivity. Investigations using the Aquarius and TRMM 3B42 matchup dataset indicate that the retrieved sea surface salinity (SSS) is underestimated by the present Aquarius algorithm compared to numerical model outputs, especially in cases of a high rain rate. For example, the bias between satellite-observed SSS and numerical model SSS is approximately 2 when the rain rate is 25 mm/h. The bias can be eliminated by accounting for rain-induced roughness, which is usually modeled by rain-generated ring-wave spectrum. The rain spectrum will be input into the Small Slope Approximation (SSA) model for the simulation of sea surface emissivity influenced by rain. The comparison with theoretical model indicated that the empirical model of rain spectrumis more suitable to be used in the simulation. Further, the coefficients of the rain spectrum are modified by fitting the simulations with the observations of the 2–year Aquarius and TRMM matchup dataset. The calculations confirm that the sea surface emissivity increases with the wind speed and rain rate. The increase induced by the rain rate is rapid in the case of low rain rate and low wind speed. Finally, a modified model of sea surface emissivity including the rain spectrum is proposed and validated by using the matchup dataset in May 2014. Compared with observations, the bias of the rain-induced sea surface emissivity simulated by the modified modelis approximately $1e^{-4}$, and the RMSE is slightly larger than $1e^{-3}$. With using more matchup data, thebias between model retrieved sea surface salinities and observationsmay be further corrected, and the RMSE may be reduced to less than 1 in the cases of low rain rate and low wind speed.

Key words: Aquarius, salinity remote sensing, rain, L-band, emissivity

Citation: Ma Wentao, Yang Xiaofeng, Yu Yang, Liu Guihong, Li Ziwei, Jing Cheng. 2015. Impact of rain-induced sea surface roughness variations on salinity retrieval from the Aquarius/SAC-D satellite. Acta Oceanologica Sinica, 34(7): 89–96, doi: 10.1007/s13131-015-0660-5

1 Introduction

Sea surface salinity (SSS) data are critical for evaluating the global evaporation minus precipitation (*E*–*P*), which is a key parameter of the global water cycle and ocean circulation studies (Terray et al., 2012). The most effective method to obtain global and long-term SSS data is satellite remote sensing. The European Space Agency launched the SMOS (Soil Moisture and Ocean Salinity mission) satellite on November 2, 2009 (Font et al., 2010; Kerr et al., 2010). Its main load is a Microwave Imaging Radiometer with Aperture Synthesis (MIRAS). Another mission was the Aquarius/SAC-D (Satellite for Scientific Applications-D) (Lagerloef et al., 2008; Le Vine et al., 2010; Yueh et al., 2010), which was undertaken by the U.S. National Aeronautics and Space Administration (NASA). These two missions have provided global SSS data over the last several years (Boutin et al., 2012; Yin et al., 2012b).

Salinity remote sensing retrieval is based on the L-band (1.4 GHz) radiometer measured sea surface brightness temperature (TB) and the Geophysical Model Function (GMF). The key to obtaining high precision SSS is the accurate simulation of the sea surface brightness temperature. In recent studies, Yin et al. (2012a; 2012b) developed the optimal sea surface emissivity model, deduced from the SMOS data, based on the two scale model and correction of the foam contribution. At the same time, Yueh et al. (2013) developed an L-band empirical brightness temperature model from the Aquarius data, which was used for wind and salinity retrieval. Additionally, Ma et al. (2014), based on the small-scale approximation (SSA) and foam model, successfully simulated the Aquarius sea surface brightness temperature.

To obtain SSS information, distributions of the sea surface temperature and wind field are needed. However, when there is rain, the sea surface becomes more complex. Rain has three main effects on salinity retrieval. First, the raindrops in atmosphere change the property of microwave radiation transmission; and it can be easily corrected in the L-band by the model developed by Wentz (2005). Second, rainfall reduces the sea surface salinity, especially in the first several centimeters related to surface stratification, while L-band radiometry can only penetrate several centimeters of sea water (Felton et al., 2014; Qu et al., 2014). Third, raindrops change the sea surface roughness. However, the latter two processes are mixed together on the sea

Foundation item: The National Natural Science Foundation of China under contract No. 41371355.
*Corresponding author, E-mail: yangxf@radi.ac.cn

surface and are difficult to separate. When the rainfall couples with wind, its influence on sea surface radiation transfer becomes more difficult to calculate. Boutin et al. (2013) found the SMOS observed sea surface freshening is linearly correlated to the SSM/I rain rate, with an estimated slope of –0.14 psu/(mm·h^{-1}) after correction for the rain atmospheric contribution. Tang et al. (2013) analyzed the surface emissivity measured by the Aquarius L-band radiometer under rainy conditions. Boutin et al. (2014) studied the relation of rainfall with SSS retrieved by SMOS in the first centimeter of the sea surface and compared SMOS SSS with data from Argo and surface drifters in rain events. Tang et al. (2014) retrieved the SSS from Aquarius under rain conditions and performed a comparison with Argo and HYCOM data.

There is also a large amount of research on rain-induced sea surface roughness variance. Bliven et al. (1997) and Craeye et al. (1997) presented an analysis of ring-wave and scatterometer data from a water surface that was agitated by simulated rain. Contreras and Plant (2006) developed a physically based ocean surface wave model that considered rain and applied it to the study of the rain effect on surface backscatter. Sobieski et al. (2009) studied the influence of the rain drop size distribution, rain rate and frequency on sea the surface elevation variance of rain waves as well as its impact on backscatter. All of these studies reveal that the rain-induced roughness may be a non-negligible error source of salinity retrieval.

In this paper, we attempt to introduce the rain spectrum model into the SSA model to simulate the rain induced roughness effect on sea surface L-band radiation and correct the bias between SSS retrieved by Aquarius and ancillary SSS data under rainy conditions. The data used in this study are described in Section 2. The methods for simulating sea surface emissivity and the rain effects are illustrated in Section 3. The model outputs and their comparison with Aquarius are discussed in Section 4. A summary is provided in Section 5.

2 Data

2.1 *Aquarius data*

The Aquarius instrument is a combination of radiometer and scatterometer operating in the L-band (1.413 and 1.26 GHz, respectively). The radiometer has three beams. The local incidence angles of the beam center at the sea surface are 28.7°, 37.8° and 45.6°. The resolutions of these beams are 76 km×94 km for the inner beam, 84 km×120 km for the middle beam and 96 km×156 km for the outer beam. Together, the three beams can provide swath coverage of approximately 390 km. The Aquarius beam locations and resolutions are shown in Fig. 1a. Aquarius Version 2.8.1 L2 data distributed by the NASA PO.DAAC at the Jet Propulsion Laboratory (JPL) have been collected in this study. The data from January 2012 to December 2013 are used for building the model; the data from May 2014 are used for validation. The Aquarius L2 data contain ocean surface brightness temperature, sea surface temperature and wind vector data. The brightness temperature has been corrected for the influence of space radiation, Faraday rotation, and atmosphere and wind direction effects (Wentz and Le Vine, 2013). The ancillary SST data are from the NOAA OISST (Reynolds) product (Reynolds et al., 2007). The wind vector information is from the NCEP (National Centers for Environmental Prediction) numerical weather forecast model. The original OISST is a daily and 0.25°×0.25° grid product, and the original NCEP wind vector is a 6-h and 1°×1° grid product. Furthermore, the ancillary SSS data, derived from the HYCOM (US Navy HYbrid Coordinate Ocean Model) (Chassignet et al., 2009) daily averaged data-assimilative analysis, are also included in this Aquarius L2 data.

2.2 *TRMM 3B42 data*

The TRMM 3B42 rain rate data are used in this research. The time resolution is 3 h, and the spatial resolution is 0.25°×0.25°. The spatial resolution is much less than the Aquarius data. The rain rate data are from a merged product of microwave and infrared radiometers with high precision and global coverage, except for latitudes higher than 50°. The Aquarius data and TRMM data are matched when the time interval between them is less than 1.5 h, and the rain rate data are averaged in the Aquarius' field of view. The dotted lines in Fig. 1a correspond to the TRMM 3B42 grid, and the three ellipses denote the coverage of the Aquarius beams. Finally, approximately 9.5 million pairs of matchup data are collected for all three Aquarius beams. The matchup data distributions with rain rate and wind speed are shown in Fig. 1b. Because of the large amount of data, the numbers here are transformed by the log function. In this figure, the data are concentrated at moderate wind speeds and a low rain rate. It is worth to note that the data in the heavy rain condition are insufficient and that more data accumulation is required in the future.

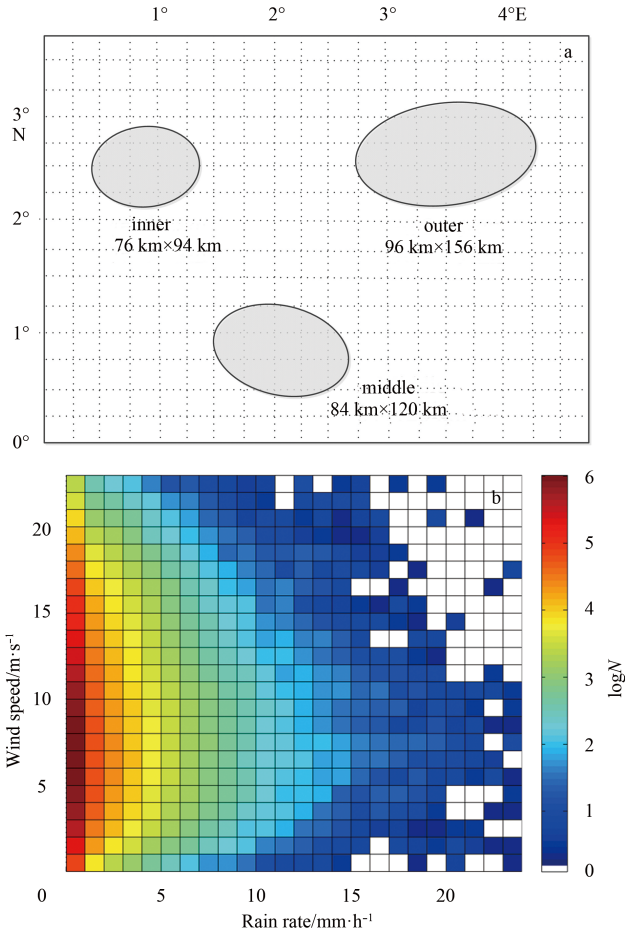

Fig. 1. Aquarius beam location and resolution on the TRMM 3B42 grid, and b. aquarius and TRMM 3B42 matchup data number as a function of rain rate and wind speed. The number in the color-bar denotes the common logarithm of matchup data number *N*. For example, log *N*=6, *N*=10^6; here, 6 means that the matchup data number *N*=10^6.

3 Methods

3.1 *Sea surface brightness temperature*

The total sea surface brightness temperature $T_{B,p}$ can be described as follows (Ma et al., 2014):

$$T_{B,P} = e_p \times T_s = (e_{p,0} + e_{p,rough}) \times T_s, \tag{1}$$

where T_s is the sea surface temperature; e_p is the total sea surface emissivity; p (p=h, v) represents the polarization; and $e_{p,0}$ is the emissivity of a calm sea surface. According to Kirchhoff's Law, the calm sea surface emissivity is expressed as (Ma et al., 2014)

$$\begin{bmatrix} e_{h,0} \\ e_{v,0} \end{bmatrix} = \begin{Bmatrix} 1 - \left| R_{hh}^{(0)}[f, \theta, \varepsilon(f, T_S, SSS)] \right|^2 \\ 1 - \left| R_{vv}^{(0)}[f, \theta, \varepsilon(f, T_S, SSS)] \right|^2 \end{Bmatrix}, \tag{2}$$

where $R_{hh}^{(0)}$ and $R_{vv}^{(0)}$ are the horizontally and vertically polarized calm surface Fresnel reflection coefficients, respectively. Furthermore, $R_{hh}^{(0)}$ and $R_{vv}^{(0)}$ are the function of radiometer frequency f, incidence angle θ and relative permittivity of sea water ε. The parameter ε is from the Debye equation with coefficients from Meissner and Wentz (2004), which are functions of SSS and T_s.

The wind-derived rough sea surface emissivity $e_{p,rough}$ is a function of the radiometer frequency f, incidence angle θ, sea surface temperature T_s, sea surface salinity SSS, 10 m-height wind speed U_{10} and wind direction WD. According to Johnson and Zhang (1999), $e_{p,rough}$ can be described by the Small Slope Approximation (SSA) model:

$$\begin{bmatrix} e_{h,rough} \\ e_{v,rough} \end{bmatrix} = -\int_0^{\infty} k_p' \mathrm{d}k_p' \int_0^{2\pi} S_W(k_p', \varphi') \begin{bmatrix} g_h(f, \theta_i, \varphi_i, \varepsilon, k_p', \varphi') \\ g_v(f, \theta_i, \varphi_i, \varepsilon, k_p', \varphi') \end{bmatrix} \mathrm{d}\varphi', \tag{3}$$

where $e_{h,rough}$ and $e_{v,rough}$ are the wind-derived rough sea surface emissivity measured in horizontal and vertical polarization, respectively. Here, e_{rough} is the integration of the sea surface wave directional spectrum S_W with the weighting function g. The sea surface wave spectrum is the function of wind speed and WD. k_p' is the sea surface wave number, and φ' is the sea surface wave direction. The double Durden-Vesecky spectrum (Durden and Vesecky, 1985) is used here. The weighting function g is the function of the frequency f, the satellite incidence angle θ_i and azimuth angle φ_i, the relative permittivity of sea water ε, the wave number k_p' and the wave direction φ'.

3.2 *Rain spectrum*

Here, the term of the rain generated ring-wave spectrum is used to denote the sea surface roughness spectrum induced by rain. When a rain drop hits a water surface, it can generate a cavity with a crown, which collapses to form a vertical stalk of water and subsides to spawn rings of gravity capillary waves that propagate outwards. An empirical form of the rainwave-number spectrum is expressed as the following log-Gaussian wave-number spectrum model (Bliven et al., 1997; Craeye et al., 1997), which is regarded as the rain spectrum 1:

$$Sk_R(k, R) = \frac{1}{2\pi} C_g(k) S_{R,peak}(R) \exp\left\{ -\pi \left[\frac{\ln \frac{f(k)}{fp}}{\frac{\Delta f}{fp}} \right]^2 \right\}, \tag{4}$$

where k is the wave number, R is the rain rate, and $f(k)$ is given by the dispersion relation,

$$\omega^2 = (2\pi f)^2 = gk + hk^3, \tag{5}$$

with g=9.8 m/s², h=74 cm³/s², C_g is the group velocity at wavenumber k, $S_{R,peak}$=6×10⁻⁴ $R^{0.53}$ cm² Hz is the amplitude of the spectral peak, f_p=5.772–0.001 8R Hz is the frequency at the peak, and Δf=4.42+0.002 8R Hz is the bandwidth.

To address the effect of rain on the sea surface, Robert and William developed a rain spectrum model based on physical theory and Ku band scatterometer data (Contreras and Plant, 2006), which is regarded as the rain spectrum 2:

$$S_R(k, R) = \left\{ \frac{64}{9} \frac{\omega^2}{g^2 k^4} \int_0^{\infty} N(D) U^3(D) D^2 \left[J_2\left(\frac{kD}{2}\right) \right]^2 \mathrm{d}D \right\} \times \left\{ \frac{1}{8\upsilon_r k^2} \left[\mathrm{e}^{-4\upsilon_r k^2 (0.2)} - \mathrm{e}^{-4\upsilon_r k^2 \tau} \right] \right\}, \tag{6}$$

$$\upsilon_r = \upsilon_0 \left[\left(1 - \mathrm{e}^{-2kd_{mix}}\right) \frac{\upsilon_e}{\upsilon_0} + \mathrm{e}^{-2kd_{mix}} \right], \tag{7}$$

where the symbols k, R, and g have the same description as rain spectrum 1, D is the rain drop diameter, the Marshall-Palmer drop size distribution is used to calculate $N(D)$, U is the terminal fall velocity of rain drop with diameter D, J_2 is the second order Bessel function of the first kind, υ_0 is kinematic viscosity, and d_{mix}=19 cm is the depth of the turbulent upper layer with the eddy viscosity υ_e=3×10⁻⁵ m²/s.

When there is rain, S_W, the sea surface wave directional spectrum induced by wind in Eq. (3) should instead be S, which is the sum of the wind-induced wave spectrum and rain-induced roughness spectrum:

$$S = S_W + S_R. \tag{8}$$

4 Calculation and discussion

Figure 2 illustrates the sea surface salinity (SSS) retrieved by Aquarius minus the SSS output from HYCOM as a function of the TRMM 3B42-derived rain rate. The rain effects are not included when retrieving these SSS data. The total number of data entries is approximately 9.5 million; the color of the scatter shows the number of the data entries. Also the number of data entries is transformed by the log function because of the large amount. The majority of data are concentrated in the area of low rain rate and low salinity of approximate 0. The difference between Aquarius SSS and HYCOM SSS becomes larger as the rain rate increases. The red line with circles shows the mean value and STD of the discrepancy. The amplitude of the mean value increases as the rain rate increases and can reach as much as 2 when the rain rate is 25 mm/h. The mean value rapidly changes when the rain rate is low and becomes more gradual as the rain rate increases. In previous studies, Boutin et al. (2013, 2014) displayed that the difference between SMOS SSS and Argo SSS linearly decreases as the rain rate increases, with a slope of approximately –0.14 per mm/h; however, only a small number of data (approximately 7 817) were used in their study. In Fig. 2, the mean value of sea surface salinity (SSS) retrieved by Aquarius minus the SSS output from HYCOM is denoted by variable y, which behaves as a function of rain rate and can be fitted by the following function:

$$y = ax^b, \tag{9}$$

where x is the rain rate, a and b are the coefficients. Using regression analysis, we obtain a=–0.42 and b=0.50. In this study, the variabley in Eq. (9) not only denotes the mean value of deference of SSSs obtained from two paths, but also represents the SSS induced by rain.

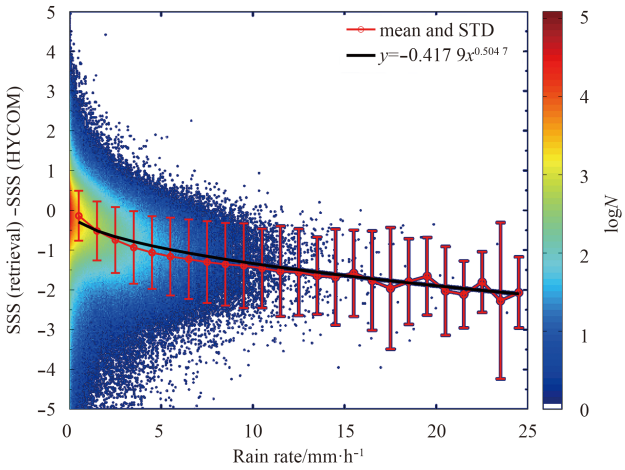

Fig. 2. The sea surface salinity (SSS) retrieved by Aquarius minus the SSS output from HYCOM as a function of the TRMM 3B42-derived rain rate. The red line with circles shows the mean value and STD of the discrepancy between the matching pair of SSS in the two datasets. The black line denotes the fitted equation, as shown in the upper-right corner. Here HYCOM is a numerical model in extensive operation. The number in the color-bar denotes the matchup data number in a log function.

Although many studies have focused on the sea surface freshening effect of rain, little is known about the influence of rain-induced roughness on sea surface emissivity. Figure 3 illustrates the omni-directional curvature spectrums for wind waves and rain-induced roughness, respectively. The wind wave spectrum shown here is calculated using the double Durden-Vesecky spectrum model (Durden and Vesecky, 1985), and the corresponding wind speed range is from 1 to 25 m/s from bottom to top. The rain-induced roughnessspectrum shown is the rain spectrum 1, calculated from Eq. (4), and the corresponding rain rate is from 1 to 25 mm/h from bottom to top. The three vertical lines represent the microwave wave number k_0=29.56 rad/m in 1.413 GHz, k_0/10 and k_0×10, respectively. The spectrum in this range will strongly influence the value of sea surface emissivity. The maximum value of the rain-induced roughness spectrum is comparable to and even higher than the wind wave spectrum for low wind speeds. When wind speed increases, the value of wind wave spectrum becomes larger than the rain-induced roughness spectrum, so the rain-induced roughness will have less impact on the sea surface during strong wind events. However, the wind curvature spectrum in Fig. 3 is non-directional. In fact, the directional wind wave spectrum in the cross-wind direction is often lower than the rain-induced roughness spectrum, which can weaken the direction signal and increase sea surface emissivity. In a previous study, Figs 1 and 6 in Tang et al. (2013) showed the weakness of the directional signal in the scatterometer and radiometer underthe condition of wind speed higher than 4.5 m/s. The NRCS (Normalized Radar Backscatter Cross Section) received by the scatterometer and the sea surface emissivity detected by the radiometer also increased when there was rain. At the same time, the change of SSS, caused by rain freshening (desalting), has less impact on the direction signal and emissivity in a well-mixed sea surface under the condition of high wind speed. Compared with rain freshening, the rain-induced roughness has a larger impact on the sea surface directional signal and emissivity under the condition of middle and high wind speed. Under the condition of heavy rain with a rate of 25 mm/h, if it is assumed that the sea water in the upperlayer (5 m depth) is well mixed with rainwater, it can be calculated that the influence of rain on the sea surface salinity is about –0.175 h^{-1}, which is a relatively small value (Boutin et al., 2014).

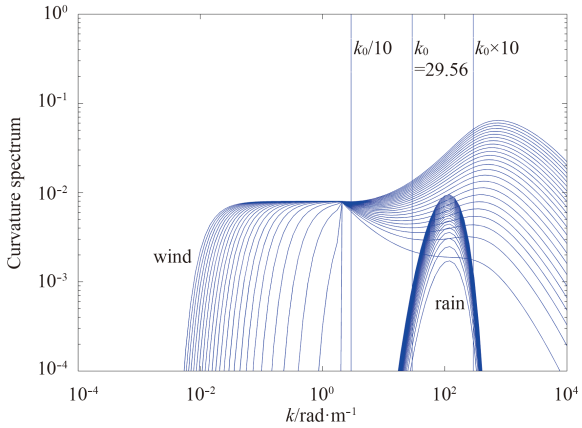

Fig. 3. Curvature spectrums induced by wind and rain, respectively, as a function of the wave number. The wind speed is from 1 to 25 m/s, with a 1 m/s bin from bottom to top. The rain rate is from 1 to 25 mm/h, with a 1 mm/h bin from bottom to top. Here k_0=29.56 rad/m is the microwave wave number in 1.413 GHz, the corresponding wavelength $\lambda=2\pi/k_0$=0.21 m.

Figure 4 shows the emissivity increment induced by rain. The sea surface emissivity is related to polarization state; here the H-polarized and V-polarized emissivity increments are denoted by solid line and dotted line, respectively. In calculation, the incidence angle is 46.29° (which corresponds to the outer beam of Aquarius), the sea surface temperature is 20°C, the sea surface salinity is 35 and the wind speed is 7.5 m/s.

In Fig. 4a, the lines without other symbols denote the satellite-observed emissivity increment caused by liquid rain water in the atmosphere, calculated from the model derived by Wentz (2005). This figure shows that this satellite-observed emissivity increases with the rain rate, the line slope in H polarization is larger than in V polarization, and the emissivity increment can reach 1.63e^{-3} (with the corresponding brightness temperature eauals 0.48 K) in H polarization and 1.17e^{-3} (with the corresponding brightness temperature equals 0.34 K) in V polarization when the rain rate is 25 mm/h.

The emissivity increment caused by rain-induced sea surface freshening, named as rain SSS H or V, is denoted by the lines with crosses in Fig. 4a. This emissivity increment is calculated by the total emissivity calculated from Eq. (1) with Aquarius SSS minus the calm sea emissivity calculated from Eq. (2) with HYCOM SSS (the bias between the two types of SSS is shown by Eq. (9)). In calculation, the wind speed isassigned to 7.5 m/s, but the effect of rain-induced sea surface roughness on emissivity is not considered. Figure 4 shows that the H-polarized emissivity is larger than the V-polarized emissivity; however, the discrepancy between two emissivity becomes small as the rain rate increases.

In Fig. 4a, the lines with triangles represent the emissivity increment induced by the rain-related sea surface roughness spectrum calculated from Eqs (3), (4) and (8); here, Eq. (4) denotes

the rain spectrum 1. The lines with circles represent the emissivity increment calculated from Eqs (3), (6) and (8); here, the Eq. (6) denotes the rain spectrum 2. Although different models of rain spectrumare used, the basic trend of emissivity increment change with rain rate is similar. The increasing rate of emissivity increment is higher in V polarization than that in H polarization.The emissivity increment is large in H polarization with a low rain rate and is large in V polarization with a high rain rate. In detail, there are some differences in the variation trend: For rain spectrum 2, the increase rate is small for low rain rates and becomes large for middle and high rain rates, while the opposite is true for rain spectrum 1. Many investigations reveal that rain can change the sea surface roughness at L-band, as observed by the scatterometer (Tang et al., 2013, 2014), so the rain-induced roughness cannot be ignored in the calculation of sea surface emissivity.

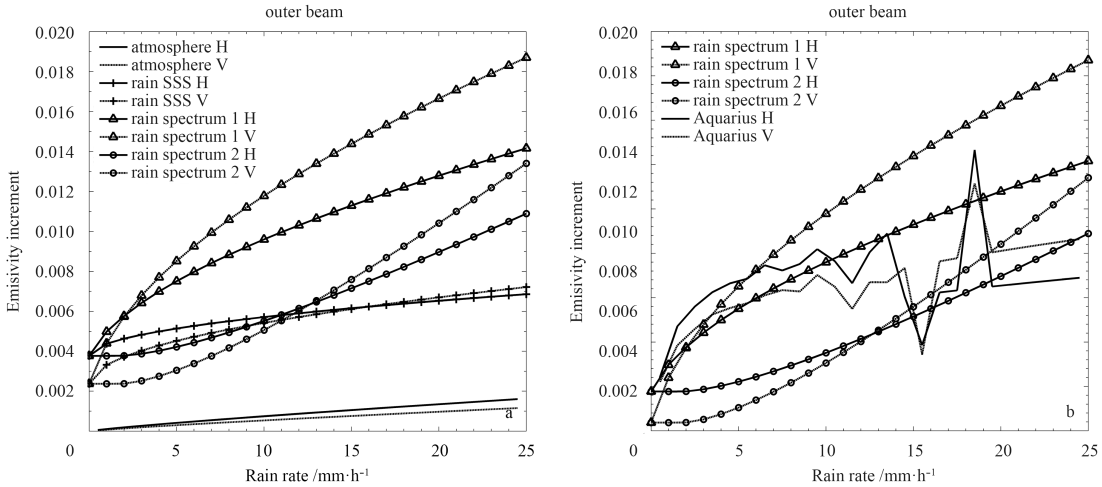

Fig. 4. The satellite-detected emissivity increment caused by the rain in the atmosphere (lines), sea surface freshening, i.e., the rain-induced SSS (lines with crosses); rain-induced roughness spectrum 1 (lines with triangles), and rain-induced roughness spectrum 2 (lines with circles) as a function of the rain rate in H polarization (solid lines) and V polarization (dotted lines); and b. the satellite-detected emissivity increment calculated by the Aquarius and TRMM 3B42 matchup dataset (lines), emissivity increment induced by rain-induced roughness spectrum 1 (lines with triangles) and rain-induced roughness spectrum 2 (lines with circles) as a function of the rain rate in H polarization (solid lines) and V polarization (dotted lines).

In Fig. 4b, the lines without symbols represent the satellite-detected emissivity increments obtained by using the Aquarius data and TRMM 3B42 matchup dataset. The solid line named as Aquarius H denotes the Aquarius-detected H-polarized emissivity increment; dotted line named as Aquarius V denotes the Aquarius-detected V-polarized emissivity increment. This increment is determined by the emissivity observed by the outer beam with rain minus that without rain but under the same conditions of wind and temperature. Figure 4b shows that this emissivity increment rises with the rain rate, the emissivity increment in H polarization is larger than that in V polarization. Both solid line and dotted line become rough like saw tooth at the high rain rate range because of insufficient data. The increase rates in both polarizations are large (small) in the low (high) rain rate range. In Fig. 4b, the lines with triangles and circles represent the emissivity increments induced by rain-related roughness spectrums 1 and 2, respectively, which are obtained using the same method as in Fig. 4a. At first, the model outputs related to spectrum 2 are substantially different from the satellite observations; thus, spectrum 2 is considered to be unsuitable for the improvement of satellite salinity retrieval algorithm. Second, we found that the increasing trend of emissivity increment calculated from the spectrum 1 model is similar to satellite observations. However, some discrepancies between them still exist. This means that spectrum 1 is more suitable for the simulation of rain-induced roughness than spectrum 2 when rain-induced freshening is not considered; and improvement of spectrum 1 based on the satellite observations is still required.

To reduce the difference between the observations and model output, the coefficients of $S_{\mathrm{R,peak}}$ in spectrum 1 are fitted using the least square method. The measured emissivity increment is averaged at a 1 mm/h interval rain rate from 0 to 25 mm/h and at a 1 m/s interval wind speed from 0 to 25 m/s. The fitted coefficients for H and V polarizationsare different because of the different performance between the model output and the Aquarius data in the two polarizations. The results are:

$$S_{\mathrm{R,peak}} = 11 \times 10^{-4} R^{0.22}, \text{in H polarization}, \tag{10}$$

$$S_{\mathrm{R,peak}} = 8 \times 10^{-4} R^{0.25}, \text{in V polarization}. \tag{11}$$

The dots in Fig. 5 show the emissivity increment, induced by rain and wind, in different beams as a function of wind speed and rain rate, which is equal to the satellite-observed emissivity minus the calm sea surface emissivity calculated from Eq. (2). The satellite-observedemissivityincrement is derived using the Aquarius sea surface brightness temperature and ancillary SST data under rainy conditions from the Aquarius and TRMM 3B42 matchup dataset. In Fig. 5, the wind speed ranges from 0 to 24 m/s, the rain rate ranges from 0 to 25 mm/h, and the data are averaged in every 3 m/s interval of wind speed and 1 mm/h interval of rain rate. The dots with different colors represent the emissivityincrements averaged at different wind speed ranges. With the same rain rate, the emissivity increment increases as the wind speed increases, and the increasebecomes morerapid as the wind speed becomes larger. With the same wind speed, the emissivity increment increases as the rain rate becomes larger.

The increasing speed of the emissivity increment to the rain rate is large at a low rain rate and low speed. As the wind speeds become larger, the rain roughness has less impact on the emissivity increment. Because the matchup data are sparse at high wind speeds and rain rates, as shown in Fig. 1, the dots in that range show an irregular distribution.

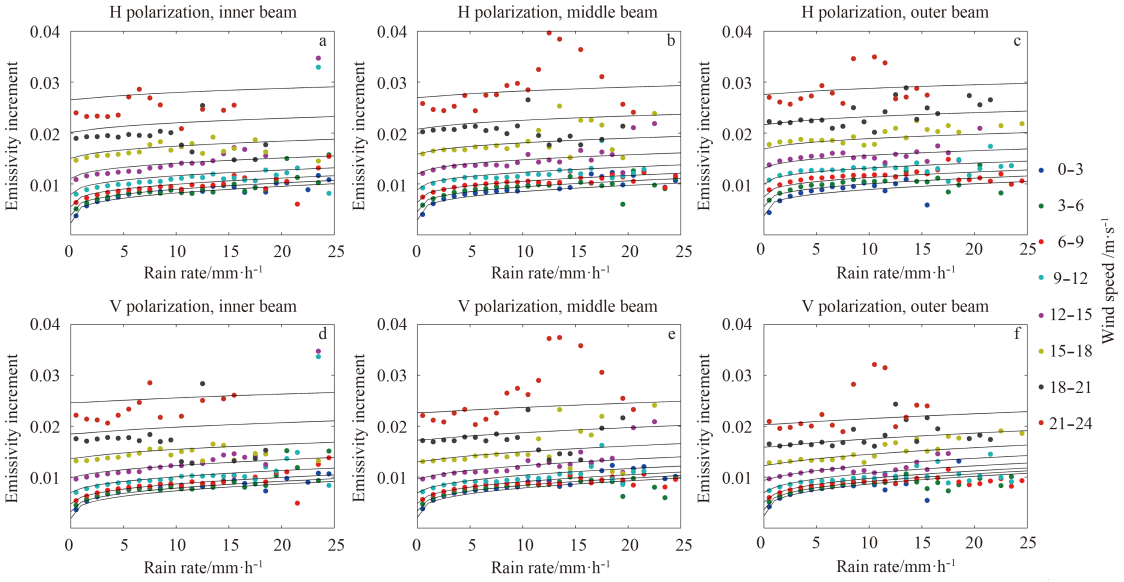

Fig. 5. The emissivity increment calculated by using the Aquarius and 3B42 matchup dataset (dots) and the modified model (lines) as a function of wind speed and rain rate. The different colors represent different wind speeds. The lines in each plot are from 1.5 to 22.5 m/s with 3 m/s bin from bottom to top.

The lines in Fig. 5 represent the emissivity increment simulated by the modified model, including Eqs (10) and (11). The model output is consistent with the Aquarius data, especially at low and moderate wind speeds and a low rain rate. There is a large discrepancy between the model output and Aquarius data at high rain rates and wind speeds, which may be caused by insufficient satellite data, as shown in Fig. 1b.

Table 1. Bias and RMSE of the emissivity increment discrepancy between the modified model output and Aquarius data

	Bias	*RMSE*
Inner H	$-4.71e^{-4}$	$2.13e^{-3}$
Middle H	$-6.91e^{-5}$	$1.82e^{-3}$
Outer H	$8.88e^{-5}$	$1.51e^{-3}$
Inner V	$9.02e^{-5}$	$2.27e^{-3}$
Middle V	$3.01e^{-4}$	$2.04e^{-3}$
Outer V	$3.40e^{-5}$	$1.49e^{-3}$

The bias and RMSE (root mean square error) of the emissivity increment discrepancy between the model output and Aquarius data are shown in Table 1. The bias between the model output and Aquarius data is approximately $1e^{-4}$, which is a very small value. The bias of the inner beam is slightly larger than the other beams in the H polarization, and the bias in middle beam is slightly larger than the other beams in the V polarization. The RMSE is slightly larger than $1e^{-3}$, which is a relatively small value as well. The RMSE decreases from the inner beam to the outer beam in both polarizations.

Finally, to validate the modified model while considering the rain roughness effect, the data of Aquarius in May 2014 were collected. Figure 6 provides the bias (solid lines) and RMSE (dotted lines) between the retrieved SSS and HYCOM SSS as a function of the rain rate (Fig. 6a) and wind speed (Fig. 6b). The lines without dots denote the bias and RMSE between the SSS retrieved without considering the rain roughness effect and the SSS from HYCOM. The lines with dots denote the bias and RMSE between the SSS retrieved considering the rain roughness effect and the SSS from HYCOM. In Fig. 6a, a large bias is found when the rain effect is not considered; the bias increases with the increasing rain rate and can be as large as 2 at high rain rates. However, the bias can be corrected when the rain roughness effect is considered in the retrieval model; the bias can be reduced to less than 0.3 when the rain rate is less than 11 mm/h. The RMSE is also reduced when the modified model is used. In Fig. 6b, the bias is also smaller than when the rain roughness is not considered. Larger error in the range of high rain rate and wind speed is found because of insufficient satellite data at that range.

In a previous study (Boutin et al., 2014), the rain effect on SMOS SSS is estimated to be between –0.18 and –0.22 psu/(mm·h^{-1}), which can cause a decrease of approximately 2 in 10 mm/hr and is consistent with the uncorrected data in this paper. A two-step data processing method was developed to correct the rain-induced roughness in their study and decreased the rain effect by only 0.01 psu/(mm·h^{-1}) and by no more than 20% in some extreme cases. However, introduction of the rain wave spectrum in this paper shows a much larger impact of the rain effect on satellite SSS, especially at low wind speeds. The bias and RMSE can be significantly corrected by the new method.

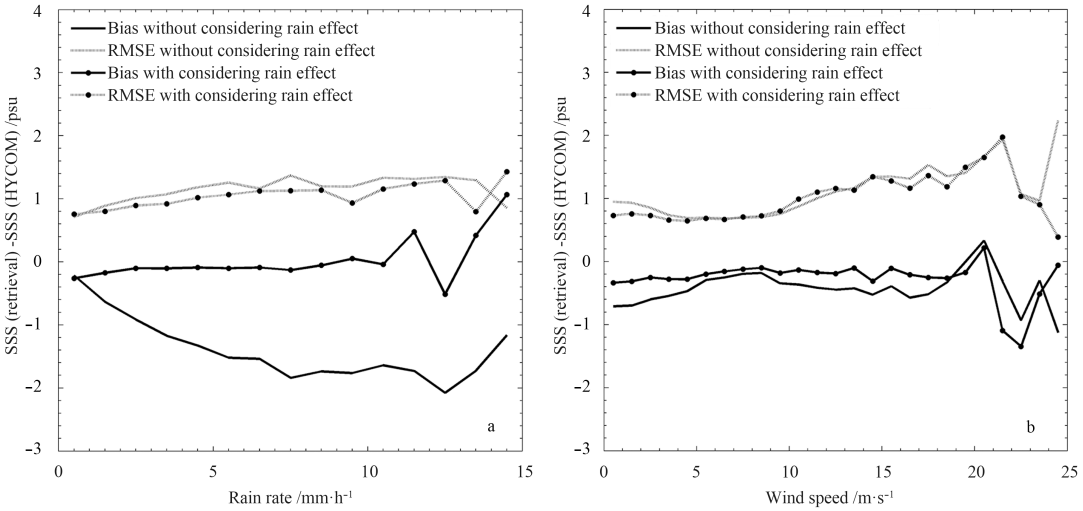

Fig. 6. Bias (solid lines) and RMSE (dotted lines) between retrieved SSS and HYCOM SSS as a function of the rain rate (a) and wind speed (b). The lines with dots are calculated considering the rain induced roughness. The lines without dots are calculated without considering the rain effects. Here HYCOM SSS data represent generally accepted and more reliable data compared to satellite data. The less bias between the retrieval model output and HYCOM SSS corresponds to a better model. Figure 6a shows clearly that the bias under rain conditions considering the rain effect is very small compared to the bias without considering rain effect.

5 Conclusions

SSS plays a significant role in the global water cycle, and satellite remote sensing helps obtain global coverage and long-term serial SSS data. However, when there is rain, a large discrepancy can be found between the SSS data retrieved by Aquarius and from the HYCOM output. The discrepancy increases with an increasing rain rate, which can reach as much as 2 in 25 mm/h. Several existing studies attribute the discrepancy to rain-induced sea surface freshness. However, the scatterometer data reveal that rain will cause an increase of sea surface roughness, which may raise sea surface emissivity as well as decrease the retrieved SSS. Until now, the influence of these two phenomena on sea surface emissivity and SSS retrieval has been very difficult to separate.

In this paper, rain wave spectrums are added into the Small Slope Approximation (SSA) model to find the contribution of rain-induced roughness to sea surface emissivity. The emissivity generated by rain-induced roughness is larger than that contributed by rain freshening and atmospheric influence. The sea surface emissivity calculated by using two models of rain wave spectrums is compared to satellite observations. It is found that rain spectrum 1 is more suitable for simulation of rain-induced roughness than rain spectrum 2; and further improvement of rain spectrum 1 can be obtained based on satellite observations.

When the rain-induced roughness is considered, a modified model of the rain wave spectrum is obtained by fitting the model coefficients to observations from the matchup dataset of Aquarius and TRMM 3B42. The satellite observations and model output with a modified spectrum show that the emissivity increment induced by rain increases with the wind speed and rain rate. The increasing speed of the emissivity increment is large at low rain rate and wind speed and is small in high rain rate and wind speed. The bias of the emissivity increment discrepancy between the model outputs and Aquarius data is approximately $1e^{-4}$; the RMSE is slightly larger than $1e^{-3}$. Finally, the model was validated by the matchup dataset in May 2014. The bias induced by rain has been corrected and the RMSE is also reduced to less than 1 at a low rain rate and wind speed. Figures 5 and 6 confirm that compared to satellite observations, the biases of sea surface emissivity and SSS retrieved by using the modified spectrum model considering the rain effect are very small compared to the biases without considering the rain effect.

Until now, the influence of rain-induced sea surface freshening on sea surface emissivity cannot be separated from rain-induced roughness, so further investigation of the rain effect on SSS retrieval is still required.

Acknowledgements

The Aquarius L2 data were provided by NASA PO.DAAC at Jet Propulsion Laboratory (http://podaac.jpl.nasa.gov/SeaSurfaceSalinity/Aquarius). The TRMM 3B42 data were provided by the U.S. Goddard Earth Sciences Data and Information Services Center (http://http://disc.sci.gsfc.nasa.gov).

References

Bliven L F, Sobieski P W, Craeye C. 1997. Rain generated ring-waves: measurements and modelling for remote sensing. IntJRemote Sens, 18(1): 221–228

Boutin J, Martin N, Reverdin G, et al. 2013. Sea surface freshening inferred from SMOS and ARGO salinity: impact of rain. Ocean Sci, 9(1): 183–192

Boutin J, Martin N, Reverdin G, et al. 2014. Sea surface salinity under rain cells: SMOS satellite and in situ drifters observations. Journal of Geophysical Research: Oceans, 119(8): 5533–5545

Boutin J, Martin N, Yin Xiaobin, et al. 2012. First assessment of SMOS data over open ocean: Part II-Sea surface salinity. IEEE Trans-Geosci Remote Sens, 50(5): 1662–1675

Chassignet E P, Hurlburt H E, Metzger E J, et al. 2009. US GODAE: global ocean prediction with the HYbrid coordinate ocean model (HYCOM). Oceanography, 22(2): 64–75

Contreras R F, Plant W J. 2006. Surface effect of rain on microwave backscatter from the ocean: Measurements and modeling. Journal of Geophysical Research: Oceans (1978–2012), 111(C8): C08019

Craeye C, Sobieski P W, Bliven L F. 1997. Scattering by artificial wind and rain roughened water surfaces at oblique incidences. IntJRemote Sens, 18(10): 2241–2246

Durden S L, Vesecky J F. 1985. A physical radar cross-section model

for a wind-driven sea with swell. IEEE JOceanic Eng, 10(4): 445–451

Felton C S, Subrahmanyam B, Murty V S N, et al. 2014. Estimation of the barrier layer thickness in the Indian Ocean using Aquarius Salinity. Journal of Geophysical Research: Oceans, 119(7): 4200–4213

Font J, Camps A, Borges A, et al. 2010. SMOS: The challenging sea surface salinity measurement from space. Proc IEEE, 98(5): 649–665

Johnson J T, Zhang Min. 1999. Theoretical study of the small slope approximation for ocean polarimetric thermal emission. IEEE Trans Geosci Remote Sens, 37(5): 2305–2316

Kerr Y H, Waldteufel P, Wigneron J-P, et al. 2010. The SMOS mission: New tool for monitoring key elements ofthe global water cycle. Proc IEEE, 98(5): 666–687

Lagerloef G, Colomb F R, Le Vine D, et al. 2008. The Aquarius/SAC-D mission: Designed to meet the salinity remote-sensing challenge. Oceanography, 21(1): 68–81

Le Vine D M, Lagerloef G S E, Torrusio S E. 2010. Aquarius and remote sensing of sea surface salinity from space. Proc IEEE, 98(5): 688–703

Ma Wentao, Yang Xiaofeng, Liu Guihong, et al. 2014. An Improved Model for L-Band Brightness Temperature Estimation Over Foam-Covered Seas Under Low and Moderate Winds. IEEE Journal of Selected Topics in Applied Earth Observations and Remote Sensing, 7(9): 3784–3793

Meissner T, Wentz F J. 2004. The complex dielectric constant of pure and sea water from microwave satellite observations. IEEE Trans Geosci Remote Sens, 42(9): 1836–1849

Qu Tangdong, Song Y T, Maes C. 2014. Sea surface salinity and barrier layer variability in the equatorial Pacific as seen from Aquarius and Argo. Journal of Geophysical Research: Oceans, 119(1): 15–29

Reynolds R W, Smith T M, Liu Chunying, et al. 2007. Daily high-resolution-blended analyses for sea surface temperature. Journal of Climate, 20(22): 5473–5496

Sobieski P, Craeye C, Bliven L F. 2009. A relationship between rain radar reflectivity and height elevation variance of ringwaves due to the impact of rain on the sea surface. Radio Science, 44(3): CiteID RS3005

Tang Wenqing, Yueh S, Fore A, et al. 2013. The rain effect on Aquarius' L-band sea surface brightness temperature and radar backscatter. Remote Sens Environ, 137: 147–157

Tang Wenqing, Yueh S H, Fore A G, et al. 2014. Uncertainty of Aquarius sea surface salinity retrieved under rainy conditions and its implication on the water cycle study. Journal of Geophysical Research: Oceans, 119(8): 4821–4839

Terray L, Corre L, Cravatte S, et al. 2012. Near-surface salinity as nature's rain gauge to detect human influence on the tropical water cycle. Journal of Climate, 25(3): 958–977

Wentz F J. 2005. The effect of clouds and rain on Aquarius salinity retrieval. Remote Sensing System Technical Memorandum, 3031805

Wentz F J, Le Vine David M. 2013. Aquarius Salinity Retrieval Algorithm. Algorithm Theoretical Basis Document

Yin Xiaobin, Boutin J, Martin N, et al. 2012a. Optimization of L-band sea surface emissivity models deduced from SMOS data. IEEE Trans Geosci Remote Sens, 50(5): 1414–1426

Yin Xiaobin, Boutin J, Spurgeon P. 2012b. First assessment of SMOS data over open ocean: Part I—Pacific Ocean. IEEE Trans Geosci Remote Sens, 50(5): 1648–1661

Yueh S H, Dinardo S J, Fore A G, et al. 2010. Passive and active L-band microwave observations and modeling of ocean surface winds. IEEE Trans Geosci Remote Sens, 48(8): 3087–3100

Yueh S H, Tang Wenqing, Fore A G, et al. 2013. L-band passive and active microwave geophysical model functions of ocean surface winds and applications to Aquarius retrieval. IEEE Trans Geosci Remote Sens, 51(9): 4619–4632